nature sustainability

Article

https://doi.org/10.1038/s41893-026-01835-6

Sea-level-driven land conversion amplified by coastal agriculture

Received: 10 July 2025

Accepted: 14 April 2026

Published online: 18 May 2026

Check for updates

Grace D. Molino[1], Yaping Chen[2] ✉, Grace C. Levins[1,3] & Matthew L. Kirwan[1]

Sea-level rise (SLR) and saltwater intrusion are driving large-scale ecosystem retreat along economically valuable coasts. However, it remains unclear how human interventions influence climate-driven processes, especially in rural areas. Sea-level-driven land use change is typically modelled as a binary response, where human-dominated uplands convert to wetlands instantaneously or else are protected indefinitely. Here we use 38 years of satellite observations across the mid-Atlantic SLR hotspot to show that marsh encroachment is nearly twice as fast, and 1.4–6.8 times more frequent, on agricultural land than forestland. Field measurements indicate that local interventions have slowed the loss of agricultural land on private property to rates far lower than SLR; however, our results suggest that, at the regional scale, agriculture accelerates the impacts of saltwater intrusion. These results imply a unique scale-dependent impact of humans on coastal management and extend our understanding of humans as principal agents of change, even in rural landscapes.

Human interventions can either exacerbate or mediate the impacts of climate change on fundamental, natural processes. Prominent examples from terrestrial landscapes include the interaction between climate and management in fire and river flow regimes[1,2]. Fire patterns historically deviated from those expected based on climate drivers alone[3] in both Europe and North America where decades of fire suppression policies reduced predicted fire frequency and burned area[3–5]. Similarly, the natural variability of river flow regimes dictated by climate is moderated by an estimated 2.8 million dams worldwide[6], which can both amplify and mediate downstream flow regimes depending on timescale and season[7]. Fires, floods and water shortages elevate the need to understand and manage how humans regulate the impacts of climate change on fundamental, natural processes.

Understanding of the role of human activities as mediators or amplifiers of climate change in coastal ecosystems is especially important given their coastal hazard mitigation potential, economic importance and priority for habitat restoration. Anthropogenic activities are well known to influence the evolution of highly developed coasts, including subsiding megacities and eroding sandy beaches[8,9]. However, sea-level rise (SLR) and saltwater intrusion are especially prominent along low-lying, rural coasts where freshwater ecosystems are rapidly converting to estuarine and saline wetlands[10–12]. More than 10,000 km^2 of coastal forested wetlands in the North American coastal plain transitioned to scrub-shrub or marsh habitats from 1996 to 2016[12], and an additional 17,000 km^2 of terrestrial and forested wetlands in the continental USA are at risk of conversion to saline wetlands with 1.5 m of SLR[13]. Modelled responses of anthropogenic land uses in rural areas are often simplified based on contradictory assumptions: either the land responds like forested areas and converts instantaneously, or humans defend anthropogenic land uses and prevent conversion to marsh completely (for example, refs. 14,15).

Despite calls to include a dynamic human role in models of coastal landscape evolution[16], developed land uses are often simply removed from predictions of sea-level-driven land conversion, as the economic value is presumed to spur the implementation of flood defence strategies[17–19]. This approach may be reasonable in major cities, where dikes, storm surge barriers and extensive pump systems protect heavily developed areas[20–22]. However, rural areas dominated by agricultural land uses are often not in the conversation about future flood infrastructure[23,24], and there are indications that attempts to defend

[1]Virginia Institute of Marine Science, William & Mary, Gloucester Point, VA, USA. [2]School of Ecology, Shenzhen Campus of Sun Yat-sen University, Shenzhen, China. [3]Department Geosciences, Union College, Schenectady, NY, USA. ✉e-mail: chenyp96@mail.sysu.edu.cn

https://doi.org/10.1038/s41893-026-01835-6

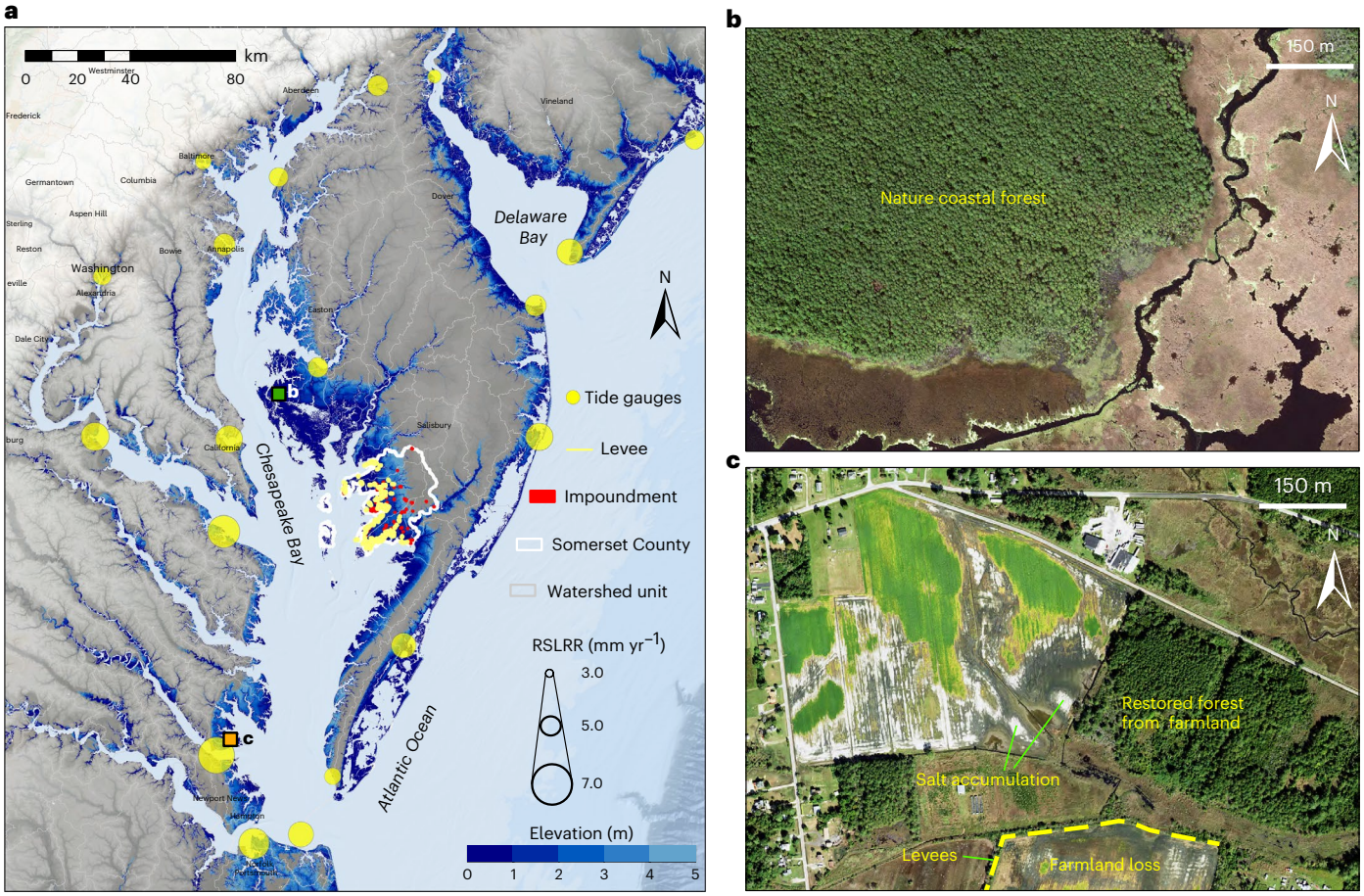

Fig. 1 | SLR and coastal salinization along the mid-Atlantic USA. a–**c**, Map of coastal land cover and land use change for the US mid-Atlantic. **a**, Yellow circles correspond to the locations of long-term tide gauges ($n = 19$), scaled by observed RSLRR between 1984 and 2022. Field sites are located in Somerset County, MD, outlined in white, where human-made levees (yellow lines) and impoundments (red areas) are manually delineated. See Extended Data Fig. 5 for an expanded view of levee and impoundment locations. The dark-green square (38.41° N, 76.22° W) and the orange square (37.28° N, 76.42° W) in **a**, respectively, correspond to typical examples of retreating upland forest (**b**) and salt-intruded farmland (**c**). All high-resolution aerial images are acquired during 2020 from NAIP. All elevations are relative to NAVD88, which approximates the mean sea level in the region[57]. Ocean basemap data in **a**, Esri, GEBCO, Garmin, FAO, NOAA, USGS. Credit: **b**,**c**, US Department of Agriculture, Farm Service Agency.

individual agricultural fields can increase their susceptibility to SLR and saltwater intrusion[25,26].

Here, we use a combination of remote sensing and field measurements from the mid-Atlantic SLR hotspot[27] to quantify differences in the rate of sea-level driven losses of human-dominated (agricultural) and largely natural (forested) sections of the coast. We show that previously unmapped, small flood defence structures on individual farms can mediate saltwater intrusion locally, but that agricultural land use ultimately amplifies the impact of SLR at the regional scale.

Results

Spatial patterns of farmland conversion to marsh

We used Landsat satellite imagery (30-m resolution) spanning almost 40 years to create a map of coastal land cover and land use change for the US mid-Atlantic (Fig. 1), a region known as a hotspot for SLR (Extended Data Table 1), coastal flooding and ecosystem shifts[27–29]. Between 1984 and 2022, 101.1 km^2 of low-lying farmland (within 2 m of sea level; Extended Data Table 2) in the Chesapeake and Delaware Bay watersheds was lost to SLR and saltwater intrusion (Fig. 2), as indicated by conversion to marsh, open water or sandy shorelines (Extended Data Table 2). These estimates are likely conservative as they do not include conversion of farmland to other land uses (that is, urbanization or reforestation) that would otherwise be replaced or partially encroached by rapidly transgressing marshes or shorelines, nor losses at slightly higher elevations that together have resulted in the loss of 557.4 km^2 of farmland between 0 m and 5 m above sea level. Agricultural losses (101.1 km^2; Fig. 2a) are similar to but lower than forest losses (235.7 km^2; Extended Data Fig. 1) from 1984 to 2020 in the same region[29]. However, it is important to recognize that the overall area of farmland loss was 14.8%, while the area of forest loss was 12.8%, even with farmland distribution skewed to higher elevations less prone to saltwater intrusion (Fig. 2c). Moreover, the proportion of land conversion for a given elevation was 1.4–6.8 times greater for agricultural land than forestland (Fig. 2). While the cumulative areal loss of forestland plateaued with increasing elevation at ~1.5 m, the cumulative loss of farmland continued to increase with higher elevations (Fig. 2b). The overwhelming majority of sea-level-driven land conversion of farmland and forest resulted in the formation of new marsh (95.2% and 94.9%, respectively)[29].

Yet, conventional reliance on lateral ecosystem extent may mask more subtle drivers of land cover change, including anthropogenic influences. To mediate the strong topographic imprint on lateral ecosystem extent, we calculated the vertical distance that farmland retreated (Extended Data Fig. 2). Averaged across the entire mid-Atlantic region, we find that the seaward boundary of agricultural land (that is, the marsh-farm boundary) retreated upslope from an elevation of 0.74 m North American Vertical Datum 1988 (NAVD88) in 1984 to an elevation of 0.87 m NAVD88 in 2022. The seaward

https://doi.org/10.1038/s41893-026-01835-6

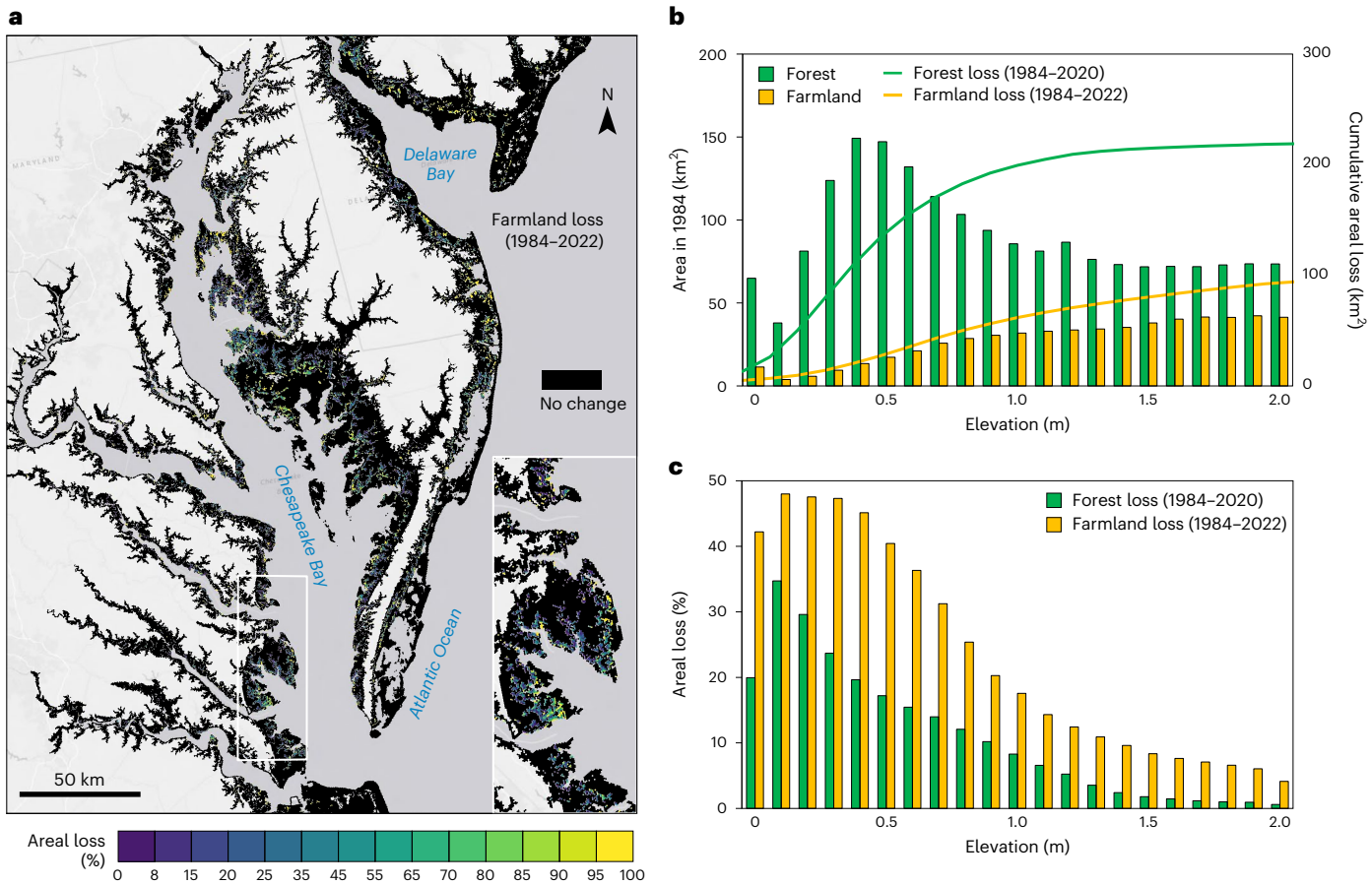

Fig. 2 | Frequency of upland conversion to wetland in forestland and farmland. **a**, Percentage loss of farmland (1984–2022). Areal losses are calculated from differenced land cover maps after excluding all changes caused by direct human activities and are shown at 0.075 km^2 resolution. **b**, Initial area and cumulative area loss of forestland (green) and farmland (yellow) along the elevation gradient. **c**, The percentage of area lost to wetlands is consistently higher in farmland (yellow bars) than that in forestland (green bars).

boundary of forestland extends to lower elevations, but retreated upslope more slowly (0.61 m to 0.69 m)[29]. Together, these findings suggest that anthropogenic (that is, agricultural) land uses intensify marsh encroachment into uplands at the regional scale.

Regional drivers of farmland retreat

We calculated vertical retreat rates of farmland that represent how the boundary between farmland and marshland moves to higher elevations through time (Extended Data Fig. 2d). This approach mediates the impact of slope on retreat rate and also produces a metric that can be directly compared with rates of SLR[29]. We aggregated spatially explicit vertical retreat rates to the scale of individual watersheds to compare how farmland and forest retreat rates varied across locations with similar physical drivers (Fig. 3 and Extended Data Fig. 3). Analysis of regional vertical farmland retreat revealed new hotspots of land conversion not observed in spatial patterns of lateral retreat (that is, southeastern Virginia) (Fig. 3b), which correspond to hotspots of relative SLR rather than slope. Within watersheds near tide gauges, farmland retreated upslope (3.22 ± 0.17 mm per year) (mean ± s.e.m.) faster than forestland (2.71 ± 0.17 mm per year), but at a rate slower than regional RSLR (4.13 - 6.74 mm per year between 1984 and 2022; Fig. 1 and Extended Data Table 1). Further examination of vertical retreat rates in a subset of watersheds with nearby tide gauges ($n = 17$) (Fig. 3d), identified relative SLR rate (RSLRR) as the primary driver of farmland vertical retreat (26%; $P < 0.05$) in a linear model ($R^2_{adj} = 0.52$) (Extended Data Fig. 4). This agrees with prior work that similarly identified RSLRR as the predominant driver of forest (43%) vertical retreat[29]. Nevertheless, our analysis shows that vertical retreat rates are not well correlated with RSLRR alone (Fig. 3d). Additional variability is explained by salinity (22%; $P < 0.05$) and soil drainage properties (9%; $P < 0.05$) (Extended Data Fig. 4). However, the linear model explains much less of the total variance in vertical retreat rate for farmland retreat (57%) than for forestland retreat (78%)[29].

Local impact of anthropogenic structures

Our finding that farmland retreat rates exceed forest retreat rates regionally, yet remain lower than RSLRRs, may reflect the historical construction of small earthen berms between the 1850s and mid-1900s to maintain arable uplands[30,31]. These small and largely unmapped levees limit the landward extent of tides, sometimes accompanying ditches in a historical ditch-bank system[30,31]. More recently, salt-impacted fields also include impoundments that consist of an enclosed earthen structure that is seasonally flooded with freshwater for recreational waterfowl hunting[32,33]. To determine whether these structural interventions effectively mediate upland conversion to marsh, we manually delineated potential barriers to saltwater intrusion on agricultural land in a small portion of the mid-Atlantic coast with extensive farmland loss (Fig. 1a, Somerset County, MD), conducted field surveys and assessed their role in the unexplained lag in vertical retreat rate with SLR.

We delineated 122 km of levees and 98 impoundments (Extended Data Fig. 5) and found that farmland without structural interventions retreated 3.45 mm per year (Fig. 4c), while farmland containing levees and impoundments retreated 2.14 mm yr^{-1} (Fig. 4b). Field surveys indicate that structural interventions are also altering

https://doi.org/10.1038/s41893-026-01835-6

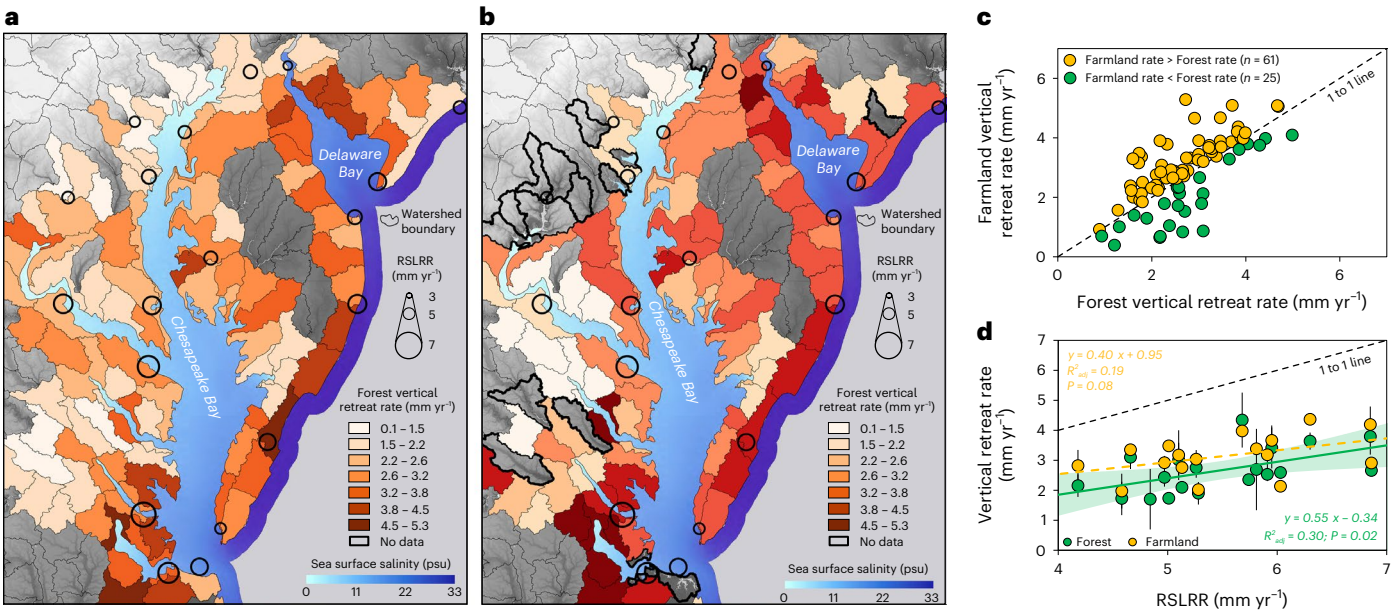

Fig. 3 | Differences in vertical retreat rates between forestland and farmland across the mid-Atlantic region. a,**b**, Vertical retreat rates are aggregated to HUC10 watershed units for forest-to-marsh conversion (**a**) and farm-to-marsh conversion (**b**). The black circles refer to RSLRR recorded by long-term tide gauges. Watersheds outlined in black are those where farmland is too sparse (<5 acres within 0–2 m elevation) for reliable quantification. **c**, Relationship between farmland and forest retreat rates, where each data point refers to an individual watershed where paired retreat rates of forestland and farmland are available. Data points above the 1-to-1 line (yellow) indicate watersheds where farmland retreat rate exceeds forestland retreat rate. **d**, Relationship between vertical retreat rates and RSLRR (linear regression analysis, two-sided test with no adjustment applied). The dashed black 1-to-1 line denotes where retreat rate equals RSLRR. The dashed yellow line represents a marginally significant trend ($0.05 \leq P < 0.1$) between farmland retreat ($n = 17$) and RSLRR, whereas the solid green line shows a significant trend ($P < 0.05$) between forest retreat ($n = 19$) and RSLRR. The green envelope refers to the 95% confidence interval. Data shown as mean ± s.d.

vegetation and soil building processes. The thickness of organic-rich wetland soils and soil organic matter content are lower behind levees than in adjacent marshes (Fig. 4e). We found low soil salinity and freshwater wetland species within the agricultural impoundment, despite low elevations that would otherwise be exposed to saltwater intrusion (Fig. 4d,e). Together, these observations reflect a disconnect from regular tidal inundation that delivers sediment and contributes to organic matter accumulation in natural marsh soils[34], and suggest that levees and impoundments locally slow the development of saline wetlands.

Discussion

Enhanced vulnerability of agricultural land

In coastal landscapes, anthropogenic responses to climate impacts have been proposed to either accelerate (that is, ditch networks[25]) or mediate (that is, dikes[17]) the conversion of agricultural uplands to marsh with SLR and saltwater intrusion[35]. Our work detected more than 101 km^2 of agricultural land that converted to marsh across the Chesapeake and Delaware Bays over nearly four decades (Fig. 2), providing an opportunity to assess the net directional influence of these contrasting human impacts over large spatial scales, and to specifically evaluate the influence of agriculture on sea-level driven ecosystem migration. Our finding that vertical retreat rates are faster in farmland than forests suggests that agriculture increases the rate of land conversion above natural rates (Fig. 3). This finding is consistent with more local observations in a Maryland county, where agricultural land was significantly more likely to convert to emergent wetlands than forested upland, even when controlling for both elevation and distance to shore[36]. Agriculture likely hastens the conversion of upland areas to marsh by replacing mature trees (that is, *Pinus taeda*) with less salt-tolerant crop species (that is, corn and soybeans)[37], resulting in a faster loss of uplands than if land cover were left in its natural forested state. Prior work demonstrated a lag between tree exposure to saltwater intrusion and tree death[29], attributed to slow carbon starvation in large, mature trees[38], which would not apply to fields planted in annual crops. Instead, common agricultural practices can increase evaporation of soil moisture, leading to increased salinities and the development of salt patches[35,37]. Finally, the mid-Atlantic coastal zone is bisected by kilometres of ditches dug in the twentieth century to drain excess water from lands intended for agriculture[11,25,35], but these may now enhance saltwater intrusion inland[25].

Previous work has highlighted the increasing vulnerability of agricultural land to SLR, including the rapid growth of salt patches[35,37]. However, our examination of rate of retreat shows that agricultural vertical retreat rates are still less than RSLRRs in all watersheds with a tide gauge present (Fig. 3b). This is reflected in the reduced explanatory power of RLSRR as a driver of farmland and forest vertical retreat rates (26% versus 43%) and the larger unexplained model variance (57% versus 78%) (Extended Data Fig. 4). Together, this suggests drivers of change unaccounted for in our model, which we attribute to heterogeneous interventions by private landowners to limit the effects of saltwater intrusion. Farmers in the mid-Atlantic have implemented practices established in drought-riddled western states to combat salinization of their fields, such as applying gypsum or spraying herbicide to combat the spread of marsh plants[35,39], interventions not captured by the land cover change analyses. Small earthen levees (Fig. 1c and Extended Data Fig. 5) are also present in former and current agricultural areas and were intended to reduce inundation[30,31]. Although it is difficult to quantify the net impact of all of these interventions, our measured retreat rates uniquely demonstrate that agricultural land conversion lags behind rates of SLR at the regional scale.

Implications for coastal management

Many models of SLR vulnerability assume that agricultural land converts to marsh instantaneously based on SLR alone[13], or else is protected and does not convert at all[19]. Binary responses may be appropriate for sections of the coast protected by large dikes maintained by

https://doi.org/10.1038/s41893-026-01835-6

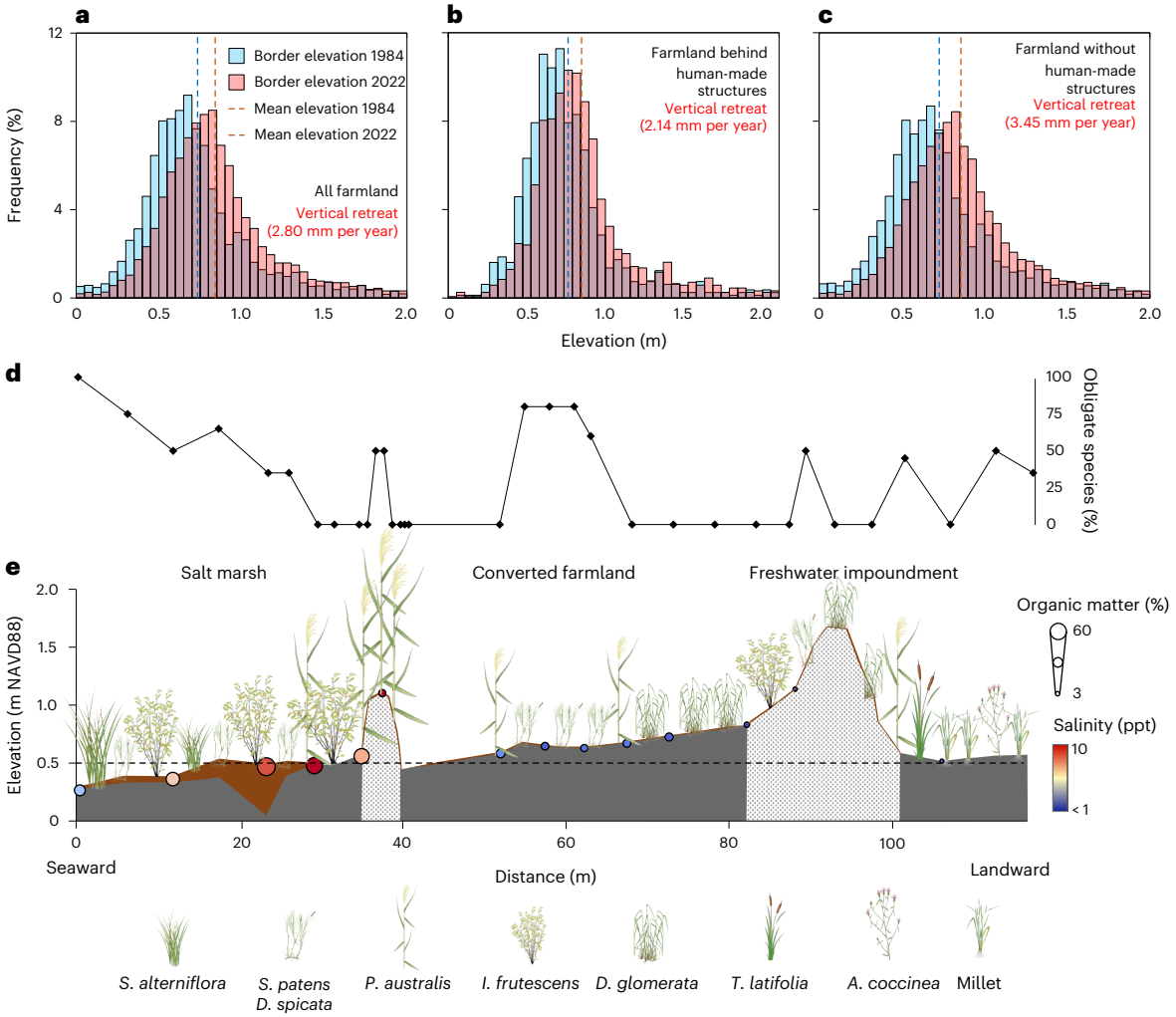

Fig. 4 | Case study of human impact on farmland conversion in Somerset County, MD. a–**c**, Histograms show shifts of marsh–farmland boundary along the elevation gradient from 1984 to 2022 with different scenarios (from left to right): all farmland in the county included (**a**), only those with levees and impoundments included (**b**) and only those with no structural interventions included (**c**). The vertical lines in each histogram correspond to the mean elevation of the marsh–farmland boundary in 1984 (dark blue) and 2022 (dark red). **d**, Percentage of obligate wetland species identified within a 0.25-m^2 plot along the transect at every point (diamond) where elevation was measured. **e**, A typical land–sea transect of coastal farmland (Goose Point; 38.16° N, −75.78° W) in the mid-Atlantic region with human-made structures identified by the dotted white areas. Simplified stratigraphy indicates mineral-rich, terrestrial soils (grey) overlain by thin organic-rich, wetland soils (brown). Elevation data are relative to NAVD88, which approximates the mean sea level in the region. Credit: icons from the University of Maryland Center for Environmental Science Integration and Application Network (https://ian.umces.edu/media-library) under a Creative Commons license CC BY-SA 4.0 (*S. alterniflora*, *P. australis*, *D. glomerata*, *T. latifolia*, *A. coccinea*, Tracey Saxby; *I. frutescens*, *S. patens*/*D. spicata*, Jane Hawkey; Millet, Jason C. Fisher, University of California Los Angeles).

government agencies, but our remote sensing and field observations suggest that small, privately maintained levees result in more subtle outcomes. We find that these small levees reduce rather than prevent land conversion, as indicated by vertical retreat rates that are close to half those of unprotected farmland (Fig. 4a–c), and the occurrence of wetland plant species located behind levees and impoundments (Fig. 4d). However, we also find that marshes on defended agricultural land function differently than natural marshes, as indicated by soils with low salinity and the presence of freshwater plants (Fig. 4e). Reduced soil organic matter thickness and lower elevation landward of the dikes could lead to the formation of open water or invasive species colonization if the levees or impoundments are breached[40]. Management recommendations are beyond the scope of our regional analysis of land use change as decisions are inherently local and depend on competing objectives (that is, preserving farmland versus conserving marshes)[33]. Nevertheless, our finding that marshes migrate more quickly into agricultural land than forestland may suggest targeting agricultural land for wetland conservation, while our finding that the construction of small-scale, privately owned levees and impoundments reduce conversion rates may suggest a way for landowners to delay agricultural land loss.

For more than 30 years, the scientific understanding of how humans influence the evolution of coastal landscapes has been dominated by the concept of 'coastal squeeze', where hardened shorelines and urban barriers lead to the loss of coastal ecosystems by preventing landward migration with SLR[41,42]. Despite perceptions of urban coasts, less than 15% of coastal watersheds in the USA are dominated by development within areas vulnerable to SLR[43]. This is consistent across the globe where traditional economic metrics justify the protection of only 13% of the global coastline. Managed or unmanaged retreat is expected for rural, often poorer coasts[44], which are assumed to convert into critical coastal wetland habitat. By contrast, our findings that privately constructed levees reduce marsh migration into agricultural land suggest a unique scale-dependent impact, where humans locally reduce the impact of saltwater intrusion, but regionally amplify it through conversion of forests to agriculture. Together, these results emphasize

that the response of ecosystems to climate change is mediated by humans even along rural coasts. Given the overwhelmingly rural nature of coastlines in the USA and globally, a paradigm shift is warranted to adequately understand the responses of these areas and the diverse priorities of the people often left out of the adaptation conversation.

Methods

Regional setting

We analysed the response of an artificially modified landscape (that is, agricultural land) to SLR and explored the efficacy of human involvement in defending coastal salinization across the US mid-Atlantic coast. The study region includes Delaware Bay and the adjacent Chesapeake Bay (roughly 12,000 km^2), covering coastal Virginia, Maryland, Delaware and New Jersey (Fig. 1 and Extended Data Table 1). This region was selected for its ideal combination of environmental conditions to test our hypotheses. First, the mid-Atlantic coast represents a known hotspot of global SLR, with RSLRR double the global average[27]. Second, forests and farmlands have been retreating landward over recent decades with strong spatial gradients in topography and RSLRR[10,36,37,45,46]. Third, the region has a long history of agricultural activities with extensive built defences (that is, levees, earthen berms and impoundment) against historical SLR visually identifiable from freely accessible high-resolution aerial imageries[30].

We computed lateral and vertical retreat rates of coastal farmland between 1984 and 2022 and compared the results against concurrent retreat rates of upland forests to evaluate potential legacy of historical land use in mediating coastal transgression with rising seas. All areas between 0 m and 5 m above sea level (relative to NAVD88, mean sea level in the region) were mapped, but all analyses were restricted to elevations between 0 m and 2 m to ensure that land use change was most directly related to SLR[47]. All elevation data are acquired from the US Geological Survey Coastal National Elevation Database (CoNED) at 1 m resolution. The observational SLR data recorded by tidal gauges (n = 19; Extended Data Table 1) are accessed from the National Oceanic and Atmospheric Administration Center for Operational Oceanographic Products and Services (https://tidesandcurrents.noaa.gov/sltrends/).

Land cover mapping

We mapped regional land cover (30 × 30 m) using cloud-free orthorectified Tier-1 Landsat surface reflectance scenes acquired in 1984 (Landsat-5 Thematic Mapper) and 2022 (Landsat-8 Operational Land Imager in 2022). The land cover maps were then analysed to compute the relative percentage of farmland and marsh across the farmland–marsh transition (as hexagon grids with side length 170 m, ~0.075 km^2) similar to ref. 29. Both land cover maps were generated by the random forest classifier in R (v. 4.1.1, packages caret and randomForest) with special focus on the marsh–farmland boundary following a similar classification algorithm described by refs. 48,37. Each of the land cover maps has five distinct classes: farmland, marsh, water, other uplands (all other upland types including forests, residential areas and impervious surface[49]) and other wetlands (all other wetland types including freshwater swamps and sandy shores[49]). Similar to the delineation of forests at the upland–wetland transition[29], here we define farmland as all cultivated lands that stretch from higher elevations completely free from saltwater flooding to low-lying, salt-intruded farmlands at the forefront of coastal transgression where crops are stressed but not yet entirely absent[37].

In brief, we acquired all Landsat images in the year of mapping during low tides over seasons of distinct plant phenological phases (spring, the greening/leaf-out season; summer, the peak growing season; and autumn, the senescent/leaf-off season)[50,51]. The multiband images were then complemented with an array of multispectral indices (normalized difference vegetation index (NDVI), enhanced vegetation index (EVI), soil adjusted vegetation index (SAVI), normalized difference water index (NDWI) and tasseled cap (TCP) brightness/greenness/wetness) computed from native Landsat scenes[52], topographical metrics (elevation, slope, topographic position index and aspect) computed from CoNED Digital Elevation Model (DEM)[29], and a set of phenology metrics (that is, the start/end/peak/length of growing season, and the base/peak/annual amplitude of NDVI) derived from the annual Landsat NDVI time series for enhanced separability between spectrally similar classes at the coastal transgression front[48]. For each land cover type, we collected ~10,000 reference sites based on field survey, drone images, high-resolution aerial images of the National Agriculture Imagery Program (NAIP) and Digital Orthophoto Quadrangle, and published data across the mid-Atlantic region[46,53–56]. The sites were randomly divided by land cover type in a 70% to 30% ratio for training and validation. For enhanced accuracy, we further processed the resulting land cover maps following the four postprocessing practices described by ref. 47 to identify and correct potential areas of misclassification. The eventual products were analysed with a confusion matrix that reached an overall classification accuracy of 92.5% (kappa coefficient 0.906) in 1984 and 95.3% (kappa coefficient 0.942) in 2022 (Extended Data Table 3).

Estimation of farmland retreat

We extracted the farmland–marsh boundary in 1984 and 2022 from the respective land cover map generated above using the methodology described previously[48]. To explore the overall extent of upward shifts of farmland–marsh boundary with rising seas between 1984 and 2022, we sampled elevation data every 100 m ('Generate Points Along Line' tool in ArcGIS v10.7) from the CoNED DEM along a smoothed farmland–marsh boundary ('Smooth Line', in ArcGIS v10.7) in 1984 and 2022. The elevation samples were carefully examined to tease apart those falling on artificially modified topography such as levees identified from CoNED DEM and high-resolution NAIP and Digital Orthophoto Quadrangle imageries. Based on the spatial patterns of farmland–marsh boundary change and the spatial configuration of coastal farmland loss, we then computed the spatially explicit rates of lateral and vertical farmland retreat as described in detail in ref. 29 that we devised earlier for reliable quantification of coastal forest retreat.

In brief, the differenced land cover maps revealed four patterns of farmland loss separated by unique arrangements of farmland–marsh boundaries (four retreat scenarios[29]). For each scenario, we generated transects cutting through the area of farmland loss at regular distance of 100 m to represent paths of farmland retreat from 1984 to 2022. For farmland loss defined by paired farmland–marsh boundaries in 1984 and 2022, the transects start from the points ('Create Perpendicular Lines', ArcGIS v10.7) generated along the boundary in 1984 and end by intersecting the opposite boundary in 2022 to signify directional retreat of farmland between our time of observation. For those outlined by a single farmland–marsh boundary (either in 1984 or 2022), a theoretical start (the area of the lowest elevation) or end (the area of the highest elevation) point was created inside the area of farmland loss according to the CoNED DEM as a measure to direct the retreat of coastal farmland over time. For these types of retreat scenarios, the paths of farmland retreat were then created by connecting the start (that is, scenario when the start of farmland retreat is unclear) or the end point (that is, scenario when the completion of farmland retreat is unclear) inside the area of farmland loss with points located on the boundary of farmland loss to simulate directional retreat of farmland from 1984 to 2022[29]. The area of farmland loss in these two scenarios is relatively small, accounting for ~7% of regional farmland loss.

We divided the length of the transect by the years of observation (1984–2022) to represent the rate of lateral farmland retreat (m per year) along each retreating path. In the same way, vertical farmland retreat rate (mm per year) of a specific path was estimated by dividing the elevation difference between the start and the end of the transect by the years in between. Finally, we generated points every 100 m along all retreating paths across the region to sample rates of farmland retreat, and the results were rasterized as hexagon grids (side length of

170 m) to explicitly quantify the spatial variability of farmland retreat ('Generate Tessellation,' ArcGIS v10.7). For hexagons outside the area of farmland loss, the retreat rates were assigned to zero corresponding to no change. A detailed description of the methodology can be found in ref. 29 for quantifying coastal forest retreat.

Field surveys

We manually delineated levees and impoundments in Somerset County, MD that were identified through 0.6-m NAIP imagery acquired in 2021 and 1-m CoNED DEM[57]. All geoprocessing was completed in ArcGIS Pro 3.2 at a spatial resolution of 1:1,500. Somerset County was chosen due to the well-documented recent agricultural land conversion to marsh[36,37,46], as well as an extensive number of levees and impoundments visible in aerial imagery[30].

We visited salt-impacted farms in Somerset County, MD, to survey levees protecting active agricultural land that were identified through our manual delineation. At each levee, we set up four transects perpendicular to the levee, ranging in length from 15 to 100 m on either side of the levee depending on site characteristics. Along each transect, we recorded vegetation and took high-precision elevation measurements with a real-time kinematic (RTK) global positioning system (GPS) every 2.5 m from the base of the levee out to 10 m on either side, and then recorded elevation every 5 m thereafter until we reached a tidal creek or dry uplands[30]. In addition, we took soil samples (10 cm depth), which were brought back to the laboratory for salinity and organic matter measurements, as well as sediment cores using a Russian peat corer to obtain organic matter thickness, every 5 m, until 20 m on either side of the levee when we switched to every 10 m. Elevation and organic matter thickness were used to understand historical levee effectiveness, while salinity, vegetation and organic matter content were proxies for modern levee effectiveness.

In the laboratory, all soil samples were weighed and dried for at least 36 h at 100 °C. Samples were weighed again to obtain soil moisture, then ground using a mortar and pestle and mechanical coffee grinder. Five grams of sample were burned at 500 °C for 8 h for loss-on-ignition. Soil salinity was measured with a salinity probe after resaturating the sample with deionized water and filtering the slurry[58].

Data analysis

We analysed environmental drivers responsible for the spatial patterns of farmland retreat with multiple linear regression models and assessed model performance with adjusted coefficient of determination (R^2_{adj}). Prior work suggests that the variables dictating vertical patterns of forest retreat differs from those shaping lateral forest retreat[29]. To explore whether similar processes exist for farmland retreat, we created two separate models: one fitted for lateral retreat rate and the other for vertical retreat rate (Extended Data Fig. 4). Before modelling, we performed a literature review to identify variables previously found relevant to patterns of coastal transgression (Extended Data Table 4). All variables are computed to the same watershed scale (HUC10 unit) accessed from the National Hydrography Dataset Plus[59]. Temporally dynamic variables (for example, RSLRR and number of hurricanes) are processed to the timespan of 1984–2022. The set of candidate variables is listed in Extended Data Table 4, which can be broadly grouped into five classes: climatic variables[12,38,47] ($n = 8$) (for example, mean annual air temperature and total annual precipitation), geophysical variables[10,45,60] ($n = 7$) (for example, elevation, mean tidal range and sea surface salinity), sea-level variables[29,61,62] ($n = 3$) (for example, RSLRR and flooding frequency), landscape metrics[63,64] ($n = 3$) (for example, patch size and proximity of patch to channels) and disturbance variables[65,66] ($n = 4$) (for example, number of tropical storms and number of hurricanes). Both models are initiated with the same set of candidate variables (Extended Data Table 4). Non-important or cross-dependent variables were eliminated one by one until a single reduced model was achieved with only significant predictors retained. All statistical analyses were performed in R (version 4.3.2). All significance was determined at the level of $P < 0.05$.

Data limitations

The spatial resolution of Landsat imagery (30 m) limits the timely detection of farmland conversion to marsh, especially in areas where the conversion occurs relatively slowly. This may result in an underestimation of farmland-to-marsh conversion, particularly in areas of recent saltwater intrusion. However, impacted land within individual parcels is often extensive (Fig. 1c), and in many cases has led to the abandonment and conversion of entire farm fields, which are inherently larger than a single Landsat pixel. The extended timespan (since 1984) of the Landsat data archive makes it ideal for observing progressive and cumulative changes that usually take decades to unfold. In addition, our field surveys conducted to validate the remote sensing results were completed at a high resolution, and showed agreement with the remotely sensed results. For example, the vegetation data that generated Fig. 4d were collected every 2.5–5 m, and the soil and salinity data that generated Fig. 4e were collected every 5–10 m.

The CoNED digital elevation model has a root mean square error of 20 cm (ref. 57). CoNED data products are specifically produced to study coastal processes in select regions of the US coastline and provide high-precision, seamless topographic information that captures nuanced vertical variations across complex coastal terrains, as demonstrated in a variety of coastal applications. The extended, multidecadal timescale of our analyses and focus on net change in elevation over time (rate) rather than absolute change offer an additional level of constraint on potential vertical uncertainties posed by the best available data.

Reporting summary

Further information on research design is available in the Nature Portfolio Reporting Summary linked to this article.

Data availability

Forest retreat rate data are available via the Environmental Data Initiative at https://doi.org/10.6073/pasta/4edf9b0d9d6660d354710748b2cf56f0. Forest cover data are available via the Environmental Data Initiative at https://doi.org/10.6073/pasta/4ae5ac3fbdb6a20dcdcb2ff36487d292. All Landsat Level-1 surface reflectance images are publicly available via the US Geological Survey EarthExplorer (https://earthexplorer.usgs.gov/) or via Google Cloud Landsat dataset (https://cloud.google.com/storage/docs/public-datasets/landsat). Watershed data were obtained from NHDPlus Version-2 data (McKay et al., 2019). Data of farmland cover change and farmland retreat rates are publicly available via the Long-Term Ecological Research Network data archive at https://doi.org/10.6073/pasta/9d195aacee6a3a3ccbf3eef7cce95d0d.

References

1. Parisien, M. A. et al. The spat ially varying influence of humans on fire probability in North America. *Environ. Res. Lett.* **11**, 075005 (2016).
2. Poff, N. L. et al. The Natural Flow Regime: a paradigm for river conservation and restoration. *Bioscience* **47**, 769–784 (1997).
3. Rogers, B. M., Balch, J. K., Goetz, S. J., Lehmann, C. E. R. & Turetsky, M. Focus on changing fire regimes: interactions with climate, ecosystems, and society. *Environ. Res. Lett.* **15**, 030201 (2020).
4. Fréjaville, T. & Curt, T. Seasonal changes in the human alteration of fire regimes beyond the climate forcing. *Environ. Res. Lett.* **12**, 035006 (2017).
5. Ruffault, J., Moron, V., Trigo, R. M. & Curt, T. Objective identification of multiple large fire climatologies: an application to a Mediterranean ecosystem. *Environ. Res. Lett.* **11**, 075006 (2016).
6. Lehner, B. et al. High-resolution mapping of the world's reservoirs and dams for sustainable river-flow management. *Front. Ecol. Environ.* **9**, 494–502 (2011).

7. Chalise, D. R., Sankarasubramanian, A. & Ruhi, A. Dams and climate interact to alter river flow regimes across the United States. *Earth's Futur.* **9**, e2020EF001816 (2021).
8. Syvitski, J. P. M. et al. Sinking deltas due to human activities. *Nat. Geosci.* **2**, 681–686 (2009).
9. McNamara, D. E. & Lazarus, E. D. in *Barrier Dynamics and Response to Changing Climate* (eds Moore, L. J. & Murray, A. B.) 363–383 (Springer, 2018); https://doi.org/10.1007/978-3-319-68086-6_12
10. Kirwan, M. L. & Gedan, K. B. Sea-level driven land conversion and the formation of ghost forests. *Nat. Clim. Chang.* **9**, 450–457 (2019).
11. O'Donnell, K. L. et al. Saltwater intrusion and sea level rise threatens U.S. rural coastal landscapes and communities. *Anthropocene* **45**, 100427 (2024).
12. White, E. E., Ury, E. A., Bernhardt, E. S. & Yang, X. Climate change driving widespread loss of coastal forested wetlands throughout the North American Coastal Plain. *Ecosystems* **25**, 812–827 (2022).
13. Osland, M. J. et al. Migration and transformation of coastal wetlands in response to rising seas. *Sci. Adv.* **8**, eabo5174 (2022).
14. Borchert, S. M., Osland, M. J., Enwright, N. M. & Griffith, K. T. Coastal wetland adaptation to sea level rise: quantifying potential for landward migration and coastal squeeze. *J. Appl. Ecol.* **55**, 2876–2887 (2018).
15. Buchanan, M. K., Kulp, S. & Strauss, B. Resilience of U.S. coastal wetlands to accelerating sea level rise. *Environ. Res. Commun.* **4**, 061001 (2022).
16. Lazarus, E. D. & Goldstein, E. B. Is there a bulldozer in your model?. *J. Geophys. Res. Earth Surf.* **124**, 696–699 (2019).
17. Enwright, N. M., Griffith, K. T. & Osland, M. J. Barriers to and opportunities for landward migration of coastal wetlands with sea-level rise. *Front. Ecol. Environ.* **14**, 307–316 (2016).
18. Hughes, M. G., Glasby, T. M., Hanslow, D. J., West, G. J. & Wen, L. Random forest classification method for predicting intertidal wetland migration under sea level rise. *Front. Environ. Sci.* **10**, 749950 (2022).
19. Warnell, K., Olander, L. & Currin, C. Sea level rise drives carbon and habitat loss in the U.S. mid-Atlantic coastal zone. *PLoS Clim.* **1**, e0000044 (2022).
20. Gotham, K. F. & Faust, M. in *Louisiana's Response to Extreme Weather* (ed. Laska, S.) 93–112 (Springer, 2020); https://doi.org/10.1007/978-3-030-27205-0_4
21. Kabat, P., Vierssen, W. van, Veraart, J., Vellinga, P. & Aerts, J. Climate proofing the Netherlands. *Nature* **438**, 283–284 (2005).
22. Ma, Z. et al. Rethinking China's new great wall. *Science* **346**, 912–914 (2014).
23. Hauer, M. E., Evans, J. M. & Mishra, D. R. Millions projected to be at risk from sea-level rise in the continental United States. *Nat. Clim. Chang.* **6**, 691–695 (2016).
24. Van Coppenolle, R. & Temmerman, S. Identifying ecosystem surface areas available for nature-based flood risk mitigation in coastal cities around the world. *Estuaries Coasts* **43**, 1335–1344 (2020).
25. Bhattachan, A. et al. Evaluating the effects of land-use change and future climate change on vulnerability of coastal landscapes to saltwater intrusion. *Elementa* **6**, 62 (2018).
26. Hingst, M. C. et al. Surface water–groundwater connections as pathways for inland salinization of coastal aquifers. *Groundwater* **61**, 626–638 (2023).
27. Sallenger, A. H., Doran, K. S. & Howd, P. A. Hotspot of accelerated sea-level rise on the Atlantic coast of North America. *Nat. Clim. Chang.* **2**, 884–888 (2012).
28. Haaf, L., Dymond, S. F. & Kreeger, D. A. Principal factors influencing tree growth in low-lying mid Atlantic coastal forests. *Forests* **12**, 1351 (2021).
29. Chen, Y. & Kirwan, M. L. Upland forest retreat lags behind sea-level rise in the mid-Atlantic coast. *Glob. Chang. Biol.* **30**, 1–14 (2023).
30. Hall, E. A., Molino, G. D., Messerschmidt, T. C. & Kirwan, M. L. Hidden levees: small-scale flood defense on rural coasts. *Anthropocene* **40**, 100350 (2022).
31. Putalik, E. & Davis, B. Bay migrations. *Places Journal* https://placesjournal.org/article/climate-and-migration-in-the-chesapeake-marsh/?cn-reloaded=1&cn-reloaded=1#0 (accessed 25 October 2022).
32. Molino, G. D. & Kirwan, M. L. Implications of waterfowl impoundments as a response to sea-level driven saltwater intrusion. *J. Environ. Manage.* **394**, 127567 (2025).
33. Sudol, T. A., Miller Hesed, C. D., Clark, J. M. & Moser, F. C. Resisting-accepting-directing sea level rise on the Chesapeake Bay: agricultural producers' motivations and actions. *J. Environ. Manage.* **332**, 117355 (2023).
34. Kirwan, M. L. & Megonigal, J. P. Tidal wetland stability in the face of human impacts and sea-level rise. *Nature* **504**, 53–60 (2013).
35. Kirwan, M. L. et al. Feedbacks regulating the salinization of coastal landscapes. *Ann. Rev. Mar. Sci.* **17**, 1–24 (2025).
36. Gedan, K. B., Epanchin-Niell, R. & Qi, M. Rapid land cover change in a submerging coastal county. *Wetlands* **40**, 1717–1728 (2020).
37. Mondal, P. et al. The spread and cost of saltwater intrusion in the US Mid-Atlantic. *Nat. Sustain*. https://doi.org/10.1038/s41893-023-01186-6 (2023).
38. McDowell, N. G. et al. Processes and mechanisms of coastal woody-plant mortality. *Glob. Chang. Biol.* **28**, 5881–5900 (2022).
39. Tully, K. et al. The invisible flood: the chemistry, ecology, and social implications of coastal saltwater intrusion. *Bioscience* **69**, 368–378 (2019).
40. Smith, J. A. M., Hafner, S. F. & Niles, L. J. The impact of past management practices on tidal marsh resilience to sea level rise in the Delaware Estuary. *Ocean Coast. Manag.* **149**, 33–41 (2017).
41. Torio, D. D. & Chmura, G. L. Assessing coastal squeeze of tidal wetlands. *J. Coast. Res.* **29**, 1049–1061 (2013).
42. Davidson, N. C. & Rothwell, P. I. Human disturbance to waterfowl on estuaries: the conservation and coastal management implications of current knowledge. *Wader Study Gr. Bull.* **68**, 97–105 (1993).
43. Holmquist, J. R., Brown, L. N. & MacDonald, G. M. Localized scenarios and latitudinal patterns of vertical and lateral resilience of tidal marshes to sea-level rise in the contiguous United States. *Earth's Fut.* **9**, e2020EF001804 (2021).
44. Lincke, D. & Hinkel, J. Economically robust protection against 21st century sea-level rise. *Glob. Environ. Chang.* **51**, 67–73 (2018).
45. Schieder, N. W., Walters, D. C. & Kirwan, M. L. Massive upland to wetland conversion compensated for historical marsh loss in Chesapeake Bay, USA. *Estuaries and Coasts* **41**, 940–951 (2018).
46. Gedan, K. B. & Fernández-Pascual, E. Salt marsh migration into salinized agricultural fields: A novel assembly of plant communities. *J. Veg. Sci.* **30**, 1007–1016 (2019).
47. Chen, Y. & Kirwan, M. L. Climate-driven decoupling of wetland and upland biomass trends on the mid-Atlantic coast. *Nat. Geosci.* **15**, 913–918 (2022).
48. Chen, Y. & Kirwan, M. L. A phenology- and trend-based approach for accurate mapping of sea-level driven coastal forest retreat. *Remote Sens. Environ.* **281**, 113229 (2022).
49. C-CAP Regional Land Cover. *NOAA Office for Coastal Management* https://coast.noaa.gov/digitalcoast/data/ccapregional.html (accessed 26 March 2025).
50. Homer, C. et al. Completion of the 2011 National Land Cover Database for the conterminous United States – representing a decade of land cover change information. *Photogramm. Eng. Remote Sens.* **81**, 345–354 (2015).

51. Campbell, A. D. & Wang, Y. Salt marsh monitoring along the mid-Atlantic coast by Google Earth Engine enabled time series. *PLoS ONE* **15**, e0229605 (2020).
52. Thomas, V. A. et al. Mapping thins to identify active forest management in southern pine plantations using Landsat time series stacks. *Remote Sens. Environ.* **252**, 112127 (2021).
53. Kirwan, M. L., Christian, R. R., Blum, L. K. & Brinson, M. M. On the relationship between sea level and *Spartina alterniflora* production. *Ecosystems* **15**, 140–147 (2012).
54. Gillen, M., Messerschmidt, T. C. & Kirwan, M. L. Shear Stress, biomass, bulk density, organic matter on the bank of the York River, VA 2018. *Environmental Data Initiative* https://doi.org/10.6073/pasta/beed4e91c44eb7297769158f60f898d4 (2021).
55. Smith, A. J., Kirwan, M. L. & Messerschmidt, T. C. Carbon stocks in forests transitioning to salt marsh at four sites in the Chesapeake Bay region, 2019. *Environmental Data Initiative* https://doi.org/10.6073/pasta/4524c22708628eb7f06d174edae89ff2 (2021).
56. Chen, Y., Messerschmidt, T. C., Smith, A. J. & Kirwan, M. L. Coastal forest aboveground biomass data at six sites in the Chesapeake Bay and Delaware Bay region, 2021. *Environmental Data Initiative* https://doi.org/10.6073/pasta/9f91ecd5fc605b27f90386d78e9077f7 (2022).
57. Danielson, J. & Tyler, D. Topobathymetric model for Chesapeake Bay Region – District of Columbia, States of Delaware, Maryland, Pennsylvania, and Virginia, 1859 to 2015. *USGS* https://topotools.cr.usgs.gov/topobathy_viewer/dwndata.htm (accessed 29 January 2020).
58. Hardie, M. & Doyle, R. in *Plant Salt Tolerance. Methods in Molecular Biology* (eds Shabala, S. & Cuin, T. A.) 415–425 (Humana Press, 2012); https://doi.org/10.1007/978-1-61779-986-0_28
59. McKay, L., Bondelid, T., Johnston, C., Moore, R. & Rea, A. *NHDPlus Version 2: User Guide (Data Model Version 2.1)* (US Environmental Protection Agency, 2012).
60. Molino, G. D., Defne, Z., Aretxabaleta, A. L., Ganju, N. K. & Carr, J. A. Quantifying slopes as a driver of forest to marsh conversion using geospatial techniques: application to Chesapeake Bay Coastal-Plain, United States. *Front. Environ. Sci.* **9**, 616319 (2021).
61. Schieder, N. W. & Kirwan, M. L. Sea-level driven acceleration in coastal forest retreat. *Geology* **47**, 1151–1155 (2019).
62. White Jr, E. & Kaplan, D. Identifying the effects of chronic saltwater intrusion in coastal floodplain swamps using remote sensing. *Remote Sens. Environ.* **258**, 112385 (2021).
63. Raabe, E. A. & Stumpf, R. P. Expansion of tidal marsh in response to sea-level rise: Gulf Coast of Florida, USA. *Estuaries Coasts* **39**, 145–157 (2016).
64. Smart, L. S. et al. Aboveground carbon loss associated with the spread of ghost forests as sea levels rise. *Environ. Res. Lett.* **15**, 104028 (2020).
65. Ury, E. A., Yang, X., Wright, J. P. & Bernhardt, E. S. Rapid deforestation of a coastal landscape driven by sea-level rise and extreme events. *Ecol. Appl.* **31**, e02339 (2021).
66. Fagherazzi, S. et al. Sea level rise and the dynamics of the marsh–upland boundary. *Front. Environ. Sci.* **7**, 25 (2019).

Acknowledgements

We are grateful for many conversations with members of the Coastal Critical Zone Network group that helped motivate this work, and to the landowners who provided us with access to their properties. We also thank the State Key Lab of Biological Control, School of Ecology, Sun Yat-Sen University for their support. G.D.M. discloses support for the research of this work from the US National Science Foundation Graduate Research Fellowship Program. Y.C. discloses support for the research and publication of this work from the Fundamental Research Funds for the Central Universities, Sun Yat-sen University (grant 77010-31610012) and the National Natural Science Foundation of China (grant 42501094). M.L.K. discloses support for the research and publication of this work from US Geological Survey Chesapeake Bay studies, the NSF Critical Zone Network (grant 2012670) and the Long-Term Ecological Research programmes (grant 1832221). G.C.L. discloses support for the research of this work from the National Science Foundation Research Experience for undergraduate students.

Author contributions

G.D.M. conceived the study, developed hypotheses, conducted the field surveys, interpreted the data and wrote the main text. Y.C. conceived the study, performed the analysis, interpreted the data and revised the manuscript. G.C.L. participated in the field surveys and contributed to the analyses. M.L.K. conceived the study, supervised the work, interpreted the data and revised the manuscript.

Competing interests

The authors declare no competing interests.

Additional information

Extended data is available for this paper at https://doi.org/10.1038/s41893-026-01835-6.

Supplementary information The online version contains supplementary material available at https://doi.org/10.1038/s41893-026-01835-6.

Correspondence and requests for materials should be addressed to Yaping Chen.

Peer review information *Nature Sustainability* thanks the anonymous reviewer(s) for their contribution to the peer review of this work.

https://doi.org/10.1038/s41893-026-01835-6

Extended Data Table 1 | Sea-level rise record by long-term tidal gauge stations across the U.S. mid-Atlantic region

NOAA Station*	Tide Gauge Identifier	Geolocation	Observation Time-span	RSLRR (mm yr^{-1})	Linear Regression
Sewells Point, VA	8638610	36.95° N, 76.33° W	1984-2022	6.21	R^2 = 0.82 (P = 2.39e-15)
Chesapeake Bay Bridge Tunnel, VA	8638863	36.97° N, 76.11° W	1984-2017	5.74	R^2 = 0.78 (P = 3.06e-12)
Kiptopeke, VA	8632200	37.17° N, 75.99° W	1984-2022	4.64	R^2 = 0.76 (P = 5.77e-13)
Yorktown, VA	8637689	37.23° N, 76.48° W	1984-2022	6.72	R^2 = 0.86 (P =2.20e-16)
Wachapreague, VA	8631044	37.61° N, 75.69° W	1984-2022	5.61	R^2 = 0.80 (P = 2.09e-14)
Dahlgren, VA	8635027	38.32° N, 77.04° W	1984-2022	5.93	R^2 = 0.84 (P = 2.46e-13)
Lewisetta, VA	8635750	37.99° N, 76.47° W	1984-2022	6.74	R^2 = 0.85 (P = 2.21e-16)
Solomons Island, MD	8577330	38.32° N, 76.45° W	1984-2022	5.81	R^2 = 0.86 (P = 2.22e-16)
Washington, D.C.	8594900	38.87° N, 77.02° W	1984-2022	4.77	R^2 = 0.60 (P = 6.32e-09)
Cambridge, MD	8571892	38.57° N, 76.06° W	1984-2022	5.02	R^2 = 0.81 (P = 4.13e-15)
Annapolis, MD	8575512	38.98° N, 76.48° W	1984-2022	5.24	R^2 = 0.77 (P = 2.35e-13)
Baltimore, MD	8574680	39.27° N, 76.58° W	1984-2022	4.52	R^2 = 0.76 (P = 3.61e-13)
Tolchester Beach, MD	8573364	39.21° N, 76.25° W	1987-2022	4.86	R^2 = 0.66 (P = 4.12e-08)
Chesapeake City, MD	8573927	39.53° N, 75.81° W	1984-2022	5.01	R^2 = 0.72 (P = 1.19e-06)
Ocean City, MD	8570283	38.33° N, 75.09° W	1984-2022	5.90	R^2 = 0.83 (P = 3.07e-13)
Lewes, DE	8557380	38.78° N, 75.12° W	1984-2022	5.26	R^2 = 0.81 (P = 7.67e-15)
Reedy Point, DE	8551910	39.56° N, 75.57° W	1984-2022	4.13	R^2 = 0.73 (P = 4.25e-12)
Cape May, NJ	8536110	38.97° N, 74.96° W	1984-2022	5.75	R^2 = 0.85 (P = 2.21e-16)
Atlantic City, NJ	8534720	39.36° N, 74.42° W	1984-2022	5.00	R^2 = 0.76 (P = 5.44e-13)

*All sea-level data are available at the NOAA Center for Operational Oceanographic Products and Services. The relative sea-level rise rate (RSLRR) is computed as the slope of linear regression between year and mean sea level.

https://doi.org/10.1038/s41893-026-01835-6

Extended Data Table 2 | Land cover change between classes from 1984 to 2022 (km^2)

Landcover in 2022		Landcover in 1984				
		Farmland	Marsh	Water	Other Uplands*	Other Wetlands#
Elevation (0-2 m)	Farmland	443.1	0.0	0.09	13.1	0. 8
	Marsh	96.3	2181.1	10.6	215.1	6.6
	Water	4.8	160.5	302.4	8.5	41.2
	Other Uplands	145.8	1.9	2.5	1769.0	6.2
	Other Wetlands	0.02	20.9	12.8	2.1	33.3
Elevation (0-5 m)	Farmland	1582.1	0.0	0.2	38.5	1.4
	Marsh	107.5	2199.2	11.0	222.0	7.6
	Water	10.6	164.7	359.3	13.5	42.6
	Other Uplands	439.0	1.9	3.8	4303.6	10.3
	Other Wetlands	0.2	21.5	13.4	2.9	54.5

*All upland types except farmland, including primary and secondary upland forest, low-lying transition forests and shrublands[48], and coastal urban areas, such as developed lands dominated by impervious surface[49]. #All wetland types after excluding marsh and water, including barren, unconsolidated sandy/silty shores, sparsely vegetated sand dunes subject to constant tidal-driven erosion and redistribution[49] and wetland forests (that is freshwater swamp).

https://doi.org/10.1038/s41893-026-01835-6

Extended Data Table 3 | Confusion matrix evaluating classification accuracy of land cover maps

Land cover maps	Land cover types	Reference data (# sites)					*User's* accuracy
		Farmland	**Marsh**	**Water**	**Other Uplands**	**Other Wetlands**	
Map in 1984	Farmland	2210	72	29	69	38	91.4%
	Marsh	66	2055	37	26	42	92.3%
	Water	21	55	2152	15	45	94.1%
	Other Uplands	86	23	26	2341	41	93.0%
	Other Wetlands	33	53	59	44	2103	91.8%
	Producer's accuracy	91.5%	91.0%	93.4%	93.8%	92.7%	
	***Overall accuracy* = 92.5%; *Kappa coefficient* = 0.9063**						
Map in 2022	Farmland	2422	44	19	32	29	95.1%
	Marsh	47	2233	22	20	32	94.9%
	Water	16	33	2098	18	24	95.8%
	Other Uplands	67	20	11	2431	17	95.5%
	Other Wetlands	20	22	38	24	2170	95.4%
	Producer's accuracy	94.2%	94.9%	95.9%	96.3%	95.5%	
	***Overall accuracy* = 95.3%; *Kappa coefficient* = 0.9417**						

https://doi.org/10.1038/s41893-026-01835-6

Extended Data Table 4 | Input variables for modeling lateral and vertical farmland retreat rate

Category	Variable	Data description	Reference*
Climatic variables	Mean annual air temperature (°C)	30-year normals of PRISM Climate Data ('PRISM Climate Group,' 2020)	Chen & Kirwan (2022a); Desantis et al. (2007); McDowell et al. (2022); Schuerch et al. (2018); White et al. (2022)
	Maximum air temperature (°C)		
	Total annual precipitation (mm)		
	Maximum vapor pressure deficit (hPa)		
	Mean annual growing degree (≥10 °C) days	Chen & Kirwan (2022a), derived from annual PRISM Climate Data ('PRISM Climate Group,' 2020)	
	Change in annual air temperature (°C) from 1984 to 2020		
	Change in annual precipitation (mm) from 1984 to 2020		
	Change in annual growing degree days from 1984 to 2020		
Geophysical variables	Elevation (meter above sea level)	CoNED DEM (Danielson et al., 2018)	Chen & Kirwan (2022a, 2022b, 2023); Chen & Ye (2014); Langston et al. (2017); Schieder et al. (2018); Smith & Kirwan (2021); Williams et al. (1998)
	Topographical slope		
	Topographic position index (unitless)		
	Sea surface salinity (psu)	Delaware Bay (Salinity Climatology for the Mid-Atlantic, 2023); Chesapeake Bay (St-Laurent et al., 2020)	
	Soil texture (unitless)	Soil properties (Walkinshaw et al., 2023)	
	Soil drainage class (unitless)		
	Mean tide range (m), computed as the difference in height between mean high water and mean low water	NOAA Tidal Datums (NOAA Tidal Datums, 2023)	
Sea level variables	Flooding frequency (0-100%) between 1984 and 2021	Global Surface Water Dataset (Pekel et al., 2016)	Chen & Kirwan (2022a, 2022b, 2023); Fagherazzi et al. (2019); Schieder & Kirwan (2019)
	Change in flooding frequency from 1984-1999 to 2000-2021		
	Relative sea-level rise rate (mm yr^{-1}) between 1984 and 2022	NOAA Tides & Currents (Center for Operational Oceanographic Products and Services, 2024)	
Landscape metrics	Mean proximity of farmland patch to channels (m)	NHDPlus Version-2 (McKay et al., 2019), and Our land cover map in 1984	Poulter, Goodall, et al. (2008); Smart et al. (2020); Ury et al. (2021)
	Mean farmland patch size (m^2)		
	Mean compactness of farmland patch (unitless)		
Disturbance variables	Number of tropical storms between 1984 and 2022	NOAA IBTrACS Project (Knapp et al., 2018)	Fagherazzi et al. (2019); Schieder & Kirwan (2019); White et al. (2022)
	Number of hurricanes between 1984 and 2022		
	Maximum inundation depth (m) by Hurricane Isabel	Storm surge simulation by ADCIRC (Molino et al., 2021)	
	Inundation duration (h) by Hurricane Isabel		

* Literatures that suggest correlation between upland retreat and the selected variables.

https://doi.org/10.1038/s41893-026-01835-6

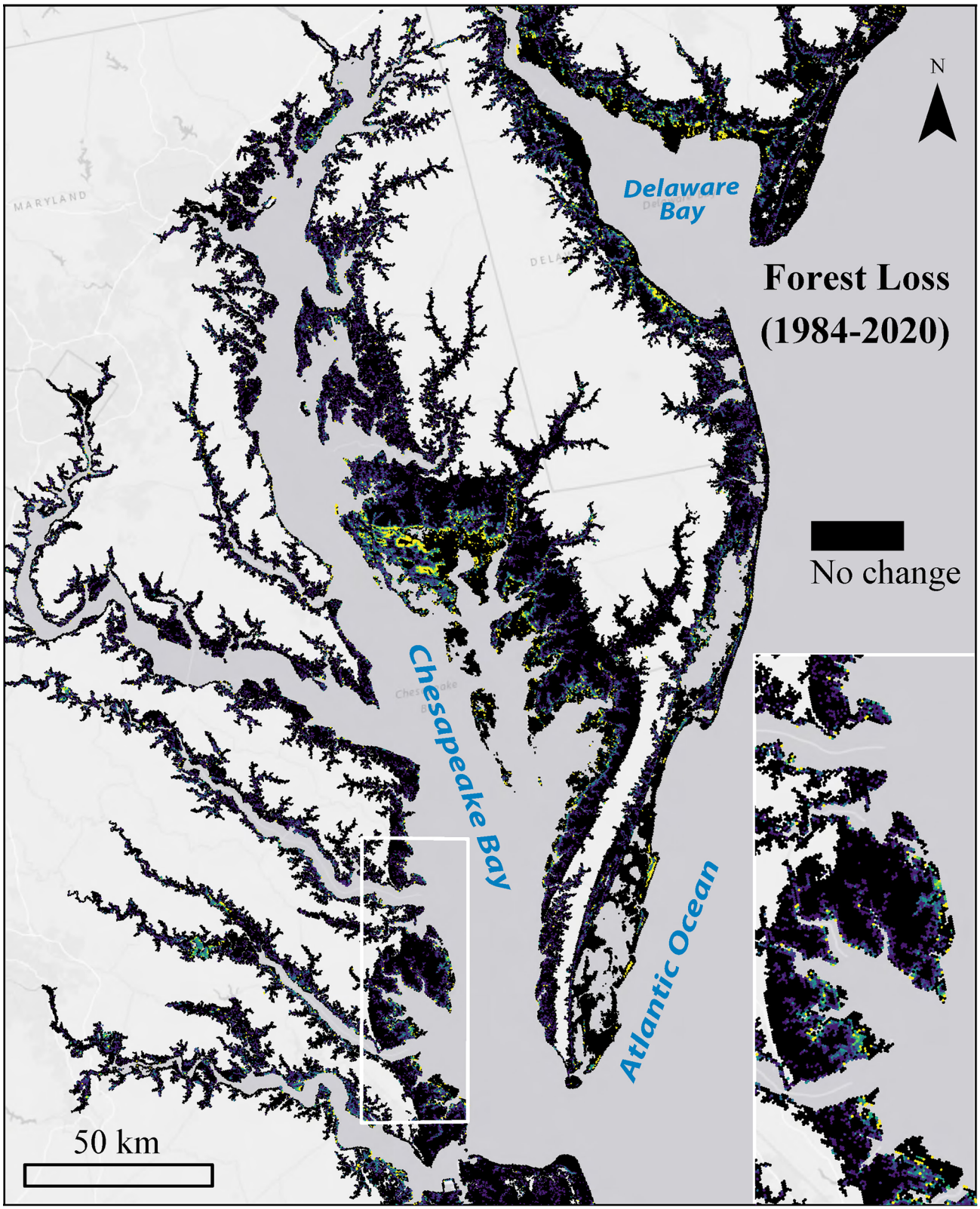

Extended Data Fig. 1 | Frequency of upland conversion to wetland in forestland. Percent areal loss of upland forests (1984-2020). Areal losses are calculated from differenced land cover maps after excluding all changes caused by direct human activities and are shown at 0.075 km^2 resolution.

https://doi.org/10.1038/s41893-026-01835-6

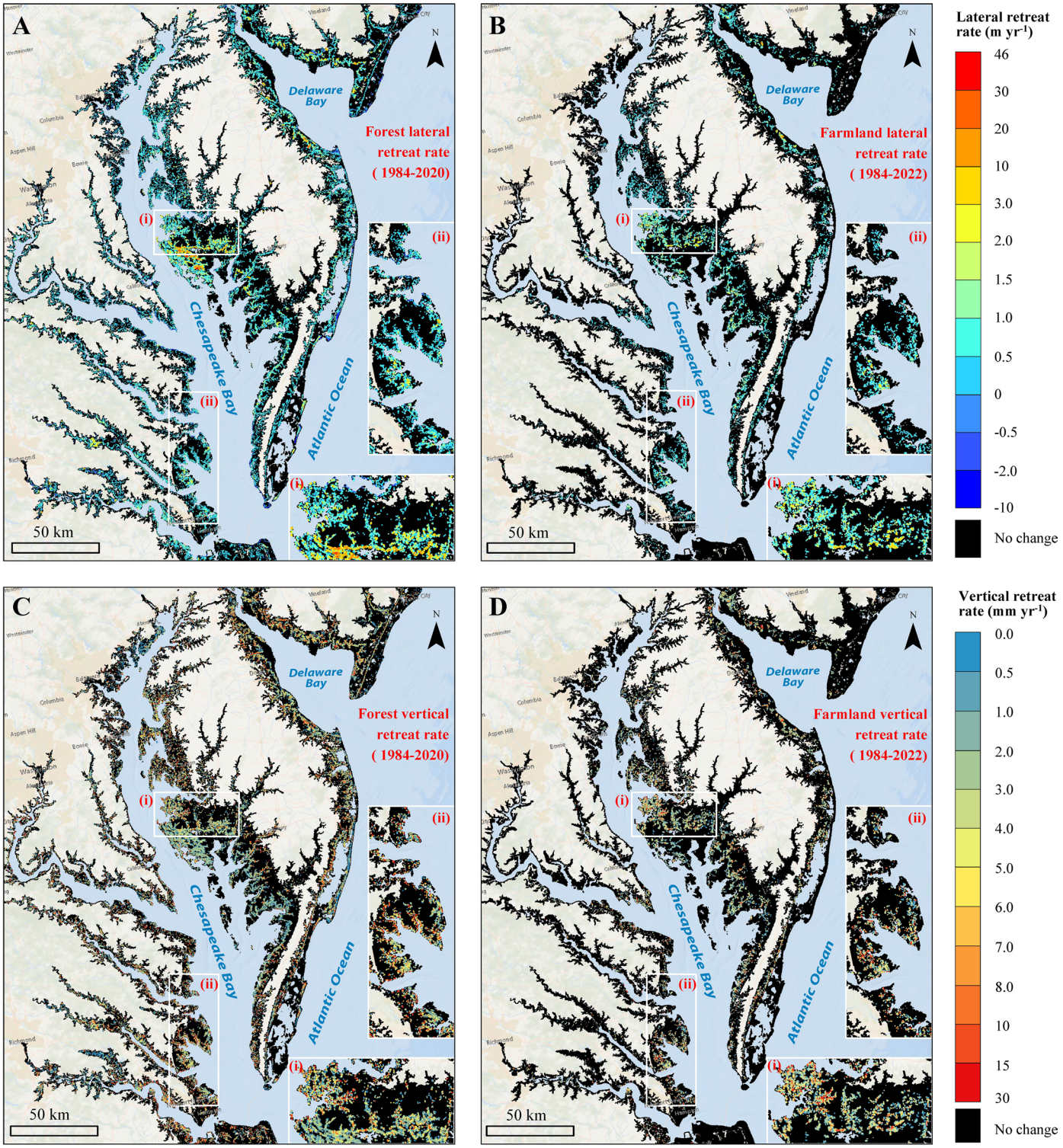

Extended Data Fig. 2 | Spatially-explicit comparison of retreat patterns between forestland and farmland. Panels in the first row show lateral retreat rate of forestland (**A**) and farmland (**B**), and panels in the second row correspond to vertical retreat rate of forestland (**C**) and farmland (**D**). Both maps are presented at the spatial resolution of 0.075 km^2. Positive values refer to landward retreat, and negative values represent seaward advance. Pixels in black indicate areas where no changes in forestland or farmland are identified after excluding all areal changes associated with human activities. Areas outlined in white (i, ii) are enlarged to the right for highlight. Elevation data are relative to NAVD88, which approximates mean sea level in the region.

https://doi.org/10.1038/s41893-026-01835-6

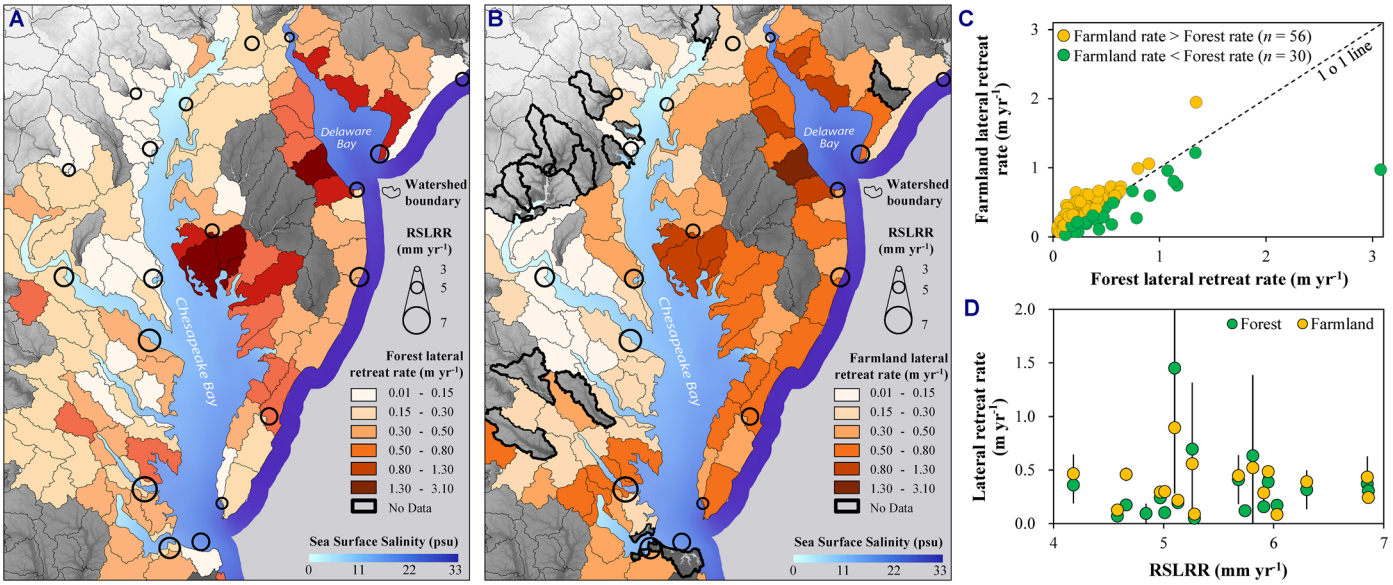

Extended Data Fig. 3 | Comparison of lateral retreat rates between forestland and farmland across the mid-Atlantic region. The pattern of watershed-scale forest retreat (**A**) shown in parallel with that of farmland retreat (**B**) (HUC10 units, NHDPlus[59]). The black circles refer to relative sea-level rise rate (RSLRR) recorded by long-term tide gauges. Watersheds outlined in black are those where farmland is too sparse (< 5 acres within 0-2 m elevation) for reliable quantification. (**C**) The lateral retreat rate of forestland (green circles) plotted against that of farmland (yellow circles). Each data point refers to a watershed where paired retreat rates of forestland and farmland are available. (**D**) No statistical relationship identified between RSLRR and lateral retreat rates of forestland (green circles, $n = 19$) or farmland (yellow circles, $n = 17$). Data shown as mean ± 1 standard deviation.

https://doi.org/10.1038/s41893-026-01835-6

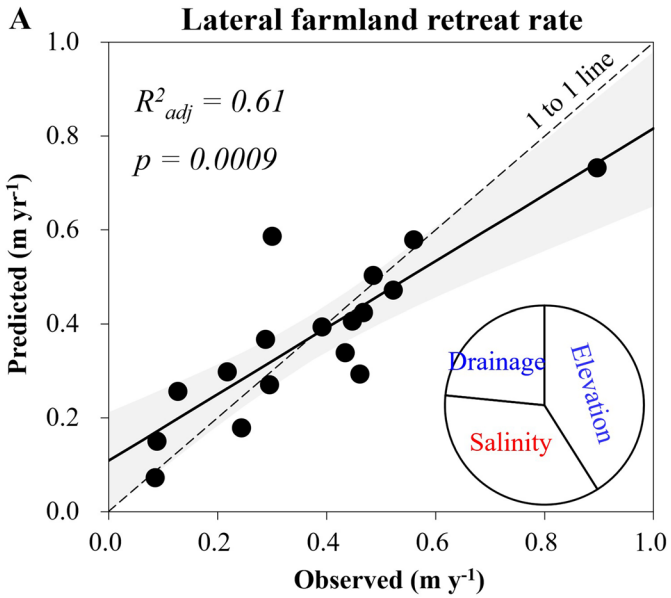

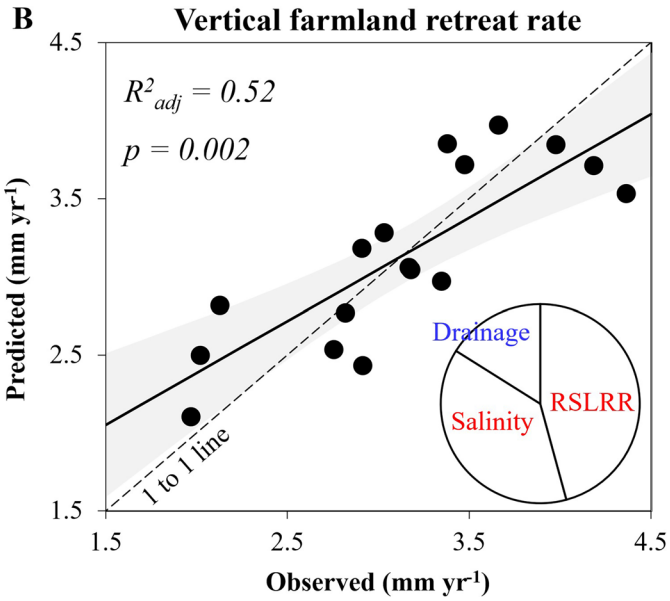

Extended Data Fig. 4 | Multiple linear regression models for spatial patterns of farmland retreat. Factors responsible for spatially-variable patterns of lateral farmland retreat (**A**) and vertical farmland retreat (**B**). The dotted lines demarcate where predicted values equal observed values. The solid lines refer to the mean linear regression trendline (two-sided test with no adjustment), bounded by the 95% confidence interval. The inserted pie charts show significant variables and their relative contribution to the overall model variance. Variables in red and blue respectively correspond to positive and negative correlation with the response variable. RSLRR is short for relative sea-level rise rate, and salinity refers to sea surface salinity.

https://doi.org/10.1038/s41893-026-01835-6

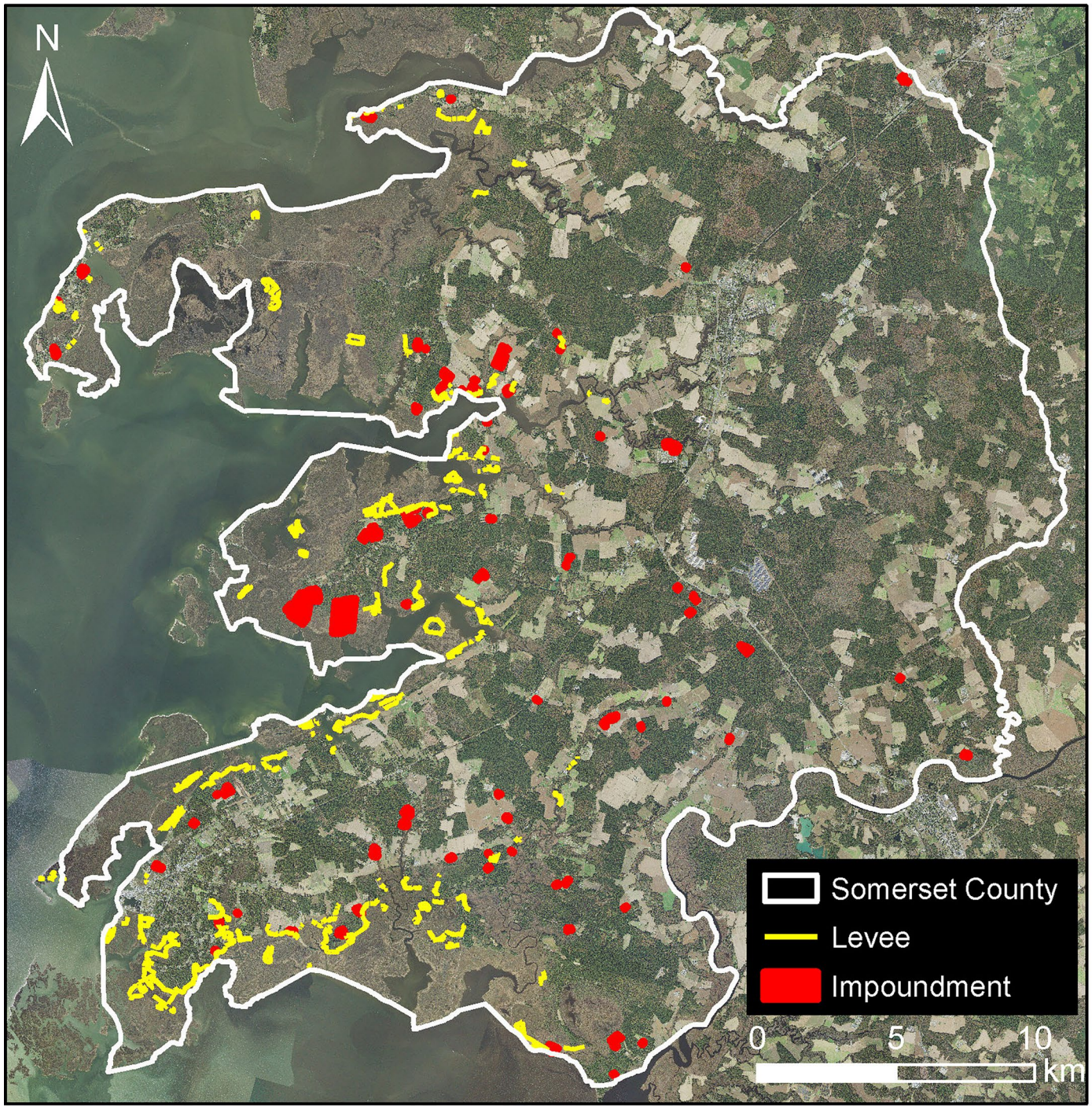

Extended Data Fig. 5 | Distribution of man-made structures in the Somerset County, MD. All high-resolution aerial images are acquired during 2020 from the National Agriculture Imagery Program (NAIP).

nature portfolio

Corresponding author(s): Yaping Chen

Last updated by author(s): Mar 21, 2026

Reporting Summary

Nature Portfolio wishes to improve the reproducibility of the work that we publish. This form provides structure for consistency and transparency in reporting. For further information on Nature Portfolio policies, see our Editorial Policies and the Editorial Policy Checklist.

Statistics

For all statistical analyses, confirm that the following items are present in the figure legend, table legend, main text, or Methods section.

n/a	Confirmed
☐	☒ The exact sample size (*n*) for each experimental group/condition, given as a discrete number and unit of measurement
☒	☐ A statement on whether measurements were taken from distinct samples or whether the same sample was measured repeatedly
☐	☒ The statistical test(s) used AND whether they are one- or two-sided *Only common tests should be described solely by name; describe more complex techniques in the Methods section.*
☒	☐ A description of all covariates tested
☒	☐ A description of any assumptions or corrections, such as tests of normality and adjustment for multiple comparisons
☐	☒ A full description of the statistical parameters including central tendency (e.g. means) or other basic estimates (e.g. regression coefficient) AND variation (e.g. standard deviation) or associated estimates of uncertainty (e.g. confidence intervals)
☐	☒ For null hypothesis testing, the test statistic (e.g. *F*, *t*, *r*) with confidence intervals, effect sizes, degrees of freedom and *P* value noted *Give P values as exact values whenever suitable.*
☒	☐ For Bayesian analysis, information on the choice of priors and Markov chain Monte Carlo settings
☒	☐ For hierarchical and complex designs, identification of the appropriate level for tests and full reporting of outcomes
☒	☐ Estimates of effect sizes (e.g. Cohen's *d*, Pearson's *r*), indicating how they were calculated

Our web collection on statistics for biologists contains articles on many of the points above.

Software and code

Policy information about availability of computer code

Data collection	Remotely sensed data (aerial data from the National Agriculture Imagery Program, and satellite data from Landsat) were analyzed using ArcGIS (version 10.8). All input images were freely available on Google Earth Engine.
Data analysis	We used R (version 4.3.2) to run the Random Forest algorithm (packages of caret and randomForest) to generate the landcover maps. Post-processing of classified images were performed in ArcMap (version 10.8). Manual delineation of barriers to migration was completed in ArcGIS Pro (version 3.2). Figures were created using Microsoft Powerpoint 2016, R (version 4.3.2), and ArcMap (version 10.8). Statistic analyses were performed in R (version 4.3.2).

For manuscripts utilizing custom algorithms or software that are central to the research but not yet described in published literature, software must be made available to editors and reviewers. We strongly encourage code deposition in a community repository (e.g. GitHub). See the Nature Portfolio guidelines for submitting code & software for further information.

Data

Policy information about availability of data

All manuscripts must include a data availability statement. This statement should provide the following information, where applicable:

- Accession codes, unique identifiers, or web links for publicly available datasets
- A description of any restrictions on data availability
- For clinical datasets or third party data, please ensure that the statement adheres to our policy

Forest retreat rate data are available at the Environmental Data Initiative (https://doi.org/10.6073/pasta/4edf9b0d9d6660d354710748b2cf56f0). Forest cover data are available at the Environmental Data Initiative (https://doi.org/10.6073/pasta/4ae5ac3fbdb6a20dcdcb2ff36487d292). All Landsat Level-1 surface reflectance images are publicly available from the United States Geological Survey EarthExplorer (https://earthexplorer.usgs.gov/) or via Google Cloud Landsat dataset (https://cloud.google.com/storage/docs/public-datasets/landsat). Watershed data were obtained from NHDPlus Version-2 data (McKay et al., 2019). Data of farmland cover change and farmland retreat rates are publicly available at the Long-Term Ecological Research Network data archive (https://doi.org/10.6073/pasta/9d195aacee6a3a3ccbf3eef7cce95d0d).

Research involving human participants, their data, or biological material

Policy information about studies with human participants or human data. See also policy information about sex, gender (identity/presentation), and sexual orientation and race, ethnicity and racism.

Reporting on sex and gender	n/a
Reporting on race, ethnicity, or other socially relevant groupings	n/a
Population characteristics	n/a
Recruitment	n/a
Ethics oversight	n/a

Note that full information on the approval of the study protocol must also be provided in the manuscript.

Field-specific reporting

Please select the one below that is the best fit for your research. If you are not sure, read the appropriate sections before making your selection.

☐ Life sciences ☐ Behavioural & social sciences ☒ Ecological, evolutionary & environmental sciences

For a reference copy of the document with all sections, see nature.com/documents/nr-reporting-summary-flat.pdf

Ecological, evolutionary & environmental sciences study design

All studies must disclose on these points even when the disclosure is negative.

Study description	This study involves analyzing freely available aerial and satellite images (in ArcGIS and R) to identify upland-wetland boundary and previously unknown barriers to marsh conversion (levees and impoundments). Soil samples were collected to measure salinity and organic matter to compare with remotely sensed data. High resolution elevation data and vegetation species and coverage were recorded where soil samples were collected.
Research sample	Six field sites were selected to cover the range in land use change from active farm fields with maintained barriers to saltwater intrusion to abandoned former fields that have been allowed to fully convert to marsh. Three of the sites were still actively farmed and had been planted with crops that season. At the other three sites the landowners had retreated further inland from the coast and were allowing the land to convert fully to marsh.
Sampling strategy	At each site we set up 4 transects perpendicular to the built barrier with soil samples (0-10 cm) taken at the same distances from the barrier along each transect so that every soil sample has 4 replicates. Where each soil sample was collected, we also recorded species present and percent cover. RTK GPS recorded precise location and elevation where each sample was collected.
Data collection	We collected 409 soil samples using a Russian peat corer. Depth of organic matter was recorded and the top 10 cm was collected to measure organic matter content and salinity in the lab. Soil samples were transported on ice back to VIMS for processing. Vegetation within a 0.25 x 0.25 m quadrat was recorded at each site where soil samples were collected. RTK GPS recorded the location and elevation of each sample collected. Dr. Grace Molino and Grace Levins conducted the field work and laboratory analyses.
Timing and spatial scale	Sample were collected over 3 months in Summer 2022. Summer was selected for peak marsh biomass to improve plant identification

Timing and spatial scale	accuracy but prior to crop harvest to minimize disruption for our sites on active farm fields. All sites were located on the Eastern Shore of Maryland and Virginia (3 per state). Transects (4 per site) were spaced a minimum of 20 m from the next nearest transect.
Data exclusions	No data were excluded from the analyses.
Reproducibility	Each sample was 1 of 4 replicates collected. Where organic matter percent or salinity of one sample exceeded the other replicates by more than one standard deviation from the replicate average, the sample was rerun to confirm. The salinity probe was recalibrated every 24 samples.
Randomization	While each transect was at least 20 m away from the next nearest transect, the overall placement of transects across the built feature was randomized.
Blinding	N/A

Did the study involve field work? ☒ Yes ☐ No

Field work, collection and transport

Field conditions	Marsh samples were collected in both high and low marsh habitats at low tide. Low marsh was typically Spartina alterniflora and high marsh was typically Spartina patens or Distichlis spicata. Tidal range in the region ranges from 0.5 to 1.4 m. Regional relative sea level rise rate is 4.13 - 6.74 mm yr-1 between 1984 and 2022. Farm field samples were collected in fields planted with either wheat or corn which are typical of the three crop rotation used in the region (wheat, corn, soy).
Location	Sites were located on the Eastern Shores of Maryland (bay side) and Virginia (lagoon side).
Access & import/export	Sites of interest were first identified by the presence of built barriers to migration that we delineated in ArcGIS. We then contacted landowners directly to obtain permission to access their property.
Disturbance	Aboveground biomass was left in place to limit disturbance to the marsh and crops. Holes from the soil collection were filled in after collection.

Reporting for specific materials, systems and methods

We require information from authors about some types of materials, experimental systems and methods used in many studies. Here, indicate whether each material, system or method listed is relevant to your study. If you are not sure if a list item applies to your research, read the appropriate section before selecting a response.

Materials & experimental systems

n/a	Involved in the study
☒	☐ Antibodies
☒	☐ Eukaryotic cell lines
☒	☐ Palaeontology and archaeology
☒	☐ Animals and other organisms
☒	☐ Clinical data
☒	☐ Dual use research of concern
☒	☐ Plants

Methods

n/a	Involved in the study
☒	☐ ChIP-seq
☒	☐ Flow cytometry
☒	☐ MRI-based neuroimaging

Plants

Seed stocks	n/a
Novel plant genotypes	n/a
Authentication	n/a